Fibrillogenesis in Continuously Spun Synthetic Collagen Fiber

Jeffrey M. Caves,[1,2] Vivek A. Kumar,[1,2] Jing Wen,[1] Wanxing Cui,[1] Adam Martinez,[1,2] Robert Apkarian,[3] Julie E. Coats,[4] Keith Berland,[4] Elliot L. Chaikof[1,2,5]

[1] Department of Surgery, Emory University, Atlanta, Georgia 30332

[2] Biomedical Engineering, Emory University, Atlanta, Georgia 30332

[3] Department of Chemistry, Emory University, Atlanta, Georgia 30332

[4] Department of Physics, Emory University, Atlanta, Georgia 30332

[5] School of Chemical and Biomolecular Engineering, Georgia Institute of Technology, Atlanta, Georgia 30322

Received 23 August 2009; accepted 16 September 2009
Published online 18 December 2009 in Wiley InterScience (www.interscience.wiley.com). DOI: 10.1002/jbm.b.31555

Abstract: The universal structural role of collagen fiber networks has motivated the development of collagen gels, films, coatings, injectables, and other formulations. However, reported synthetic collagen fiber fabrication schemes have either culminated in short, discontinuous fiber segments at unsuitably low production rates, or have incompletely replicated the internal fibrillar structure that dictates fiber mechanical and biological properties. We report a continuous extrusion system with an off-line phosphate buffer incubation step for the manufacture of synthetic collagen fiber. Fiber with a cross-section of 53 ± 14 by 21 ± 3 μm and an ultimate tensile strength of 94 ± 19 MPa was continuously produced at 60 m/hr from an ultrafiltered monomeric collagen solution. The effect of collagen solution concentration, flow rate, and spinneret size on fiber size was investigated. The fiber was further characterized by microdifferential scanning calorimetry, transmission electron microscopy (TEM), second harmonic generation (SHG) analysis, and in a subcutaneous murine implant model. Calorimetry demonstrated stabilization of the collagen triple helical structure, while TEM and SHG revealed a dense, axially aligned D-periodic fibril structure throughout the fiber cross-section. Implantation of glutaraldehyde crosslinked and non-crosslinked fiber in the subcutaneous tissue of mice demonstrated limited inflammatory response and biodegradation after a 6-week implant period. © 2009 Wiley Periodicals, Inc. J Biomed Mater Res Part B: Appl Biomater 93B: 24–38, 2010

Keywords: collagen fiber; fibrillogenesis; wet spinning; self-assembly; fibril

INTRODUCTION

Collagen serves a critical structural role in soft tissues, related organ systems, and bone, and determines a considerable range of mechanical and biological properties. Consequently, collagen-based materials have been candidates for tissue repair and replacement for decades. The collagen family consists of at least 27 known proteins characterized by triple helical macromolecular structure and their structural roles in the extracellular matrix.[1,2] All collagens consist of three peptide chains, the α-chains, containing a Gly-x-y amino acid repeat motif, where x and y are frequently proline and hydroxylated proline. The α-chains form left-handed coils that intertwine into a right-handed triple helix. This continuous rod-like region is 300 nm long and 1.5 nm in diameter in the fibril forming collagens, collagen types I, II, III, V, and IX. Two globular domains, significant for the initiation of triple helical folding, intracellular transport, and regulation of fibril assembly, flank the triple helical region of type I collagen. Enzymatic cleavage of the majority of the two globular domains reduces monomer solubility, triggering packing into ordered fibrils in a cell-directed self-assembly process.[3,4] Fibril formation can begin during intracellular transport, but is also regulated by cell surface proteins in culture, and continues through additional fibril initiation, growth, and fusion in the extracellular space.[2]

The collagen structural hierarchy begins with the monomer superhelix, and continues with microfibrils, fibrils, and a diversity of fibril organizational schemes. The microfibril structure and assembly pattern, or patterns, remains incompletely understood,[5,6] and fibrils may even be tubular with

Correspondence to: E. L. Chaikof (e-mail: echaiko@emory.edu)

an ordered periphery and a disordered or fluidic core.[7,8] Fibril compositions are tissue dependent and often heterotypic, with specific blends regulating fibril properties. For example, the addition of increasing type V collagen to type I fibrils progressively reduces fibril diameter in vitro.[9] The thin, uniform fibrils of the cornea are type I collagen with a relatively large type V fraction. Similarly, in cartilage the diameter of type II collagen fibrils is limited by the presence of type XI collagen.[10] Collagen fibrils are also associated with proteoglycans, fibril-associated collagens with interrupted triple helices, fibronectin, and other binding partners which play a variety of roles including mechanically linking fibrils, facilitating intrafibrillar slipping, and regulating fibril assembly, spacing, orientation, and diameter.[4,11]

The diversity of collagen fibril organization schemes has been categorized into those suited for uniaxial tensile loading, found in tendons and ligaments, and those adapted for multidirectional loading, observed in the blood vessel wall, cartilage, skin, and other compliant tissues.[12] In the former case, fibrils are parallel, tightly packed into fibers with diameters often in the tens of microns.[13] Fibrils in these tissues display a multimodal diameter distribution, including large fibrils of up to 500 nm. Large diameter fibrils may increase the overall strength, while smaller fibrils with greater surface area may decrease intrafibrillar slipping, reducing mechanical creep.[12] Mulitmodal diameter distribution also increases the attainable fibril packing density. In contrast, in tissues subject to biaxial or multidirectional loading, a large portion of the fibrils are more loosely packed, with smaller diameters that are more uniformly sized for a given tissue.[12]

Rapidly expanding understanding of the ECM and progress toward the generation of synthetic matrix components suggests that synthetic collagen fibers offer compelling advantages over traditional polymers for soft tissue repair and replacement. Bovine and porcine collagen have been implanted clinically for decades and are well-tolerated with a low incidence of allergic response.[14] Recent progress has led to the realization that native ECM repair scaffolds elicit fundamentally different host responses compared to other biomaterials.[15] This marked difference is due to the established dynamic and reciprocal relationship between the ECM and cellular occupants, whereby cues from the ECM influence gene expression. Consequently, the ECM is recognized as an important determinant of tissue morphogenesis, cell proliferation and differentiation, and the maintenance of homeostasis.[16] Although incomplete understanding and technical complexity currently prevent complete reverse-engineering of the ECM, several strategies for the fabrication of 3D organized collagen matrices are progressing.[17–19] Moreover, engineered collagen and elastin analogues produced by recombinant[20–22] or solid-phase synthesis[23] may soon enhance control over fibril dimensions, mechanics, and the capacity to regulate cell migration, proliferation and differentiation. Therefore, synthetic collagen fibers may be more likely than traditional polymers to reproduce the key mechanical and bioinductive aspects of native ECM.

In summary, native ECM has demonstrated clear advantages as a biomaterial for tissue repair or replacement. However, there is little opportunity to adjust the composition and microstructure of ECM, limiting the range of attainable properties. We postulate that a process for the scalable fabrication of synthetic collagen fiber from an ultra-filtered monomer solution will provide a preferred starting point for ECM engineering. In this study, we report a process in which the relatively short incubation times for efficient continuous fiber spinning were decoupled from the longer incubation required for collagen fibril self-assembly. The continuous spinning system included a fiber extrusion tube and 2 m fiber rinsing bath. After the fiber was dried, collected, and stored on carrier cylinders it was subjected to a separate off-line fibrillogenesis step. The decoupled system resulted in production of hundreds of meters of continuous fiber, with evidence of fibril self-assembly throughout the fiber cross-section.

MATERIALS AND METHODS

Isolation and Purification of Monomeric Collagen

Acid-soluble, monomeric rat-tail tendon collagen (MRTC) was obtained from Sprague-Dawley rat tails following Silver and Trelstad.[24] Frozen rat tails (Pel-Freez Biologicals, Rogers, AK) were thawed at room temperature and tendon was extracted with a wire stripper, immersed in 10 m*M* HCl (pH 2.0; 150 mL per tail) and stirred for 4 hr at room temperature. Soluble collagen was separated by centrifugation at 30,000*g* and 4°C for 30 minutes followed by sequential filtration through P8, 0.45 μm, and 0.2 μm membranes. Addition of concentrated NaCl in 10 m*M* HCl to a net salt concentration of 0.7 *M*, followed by 1 hr stirring and 1 hr centrifugation at 30,000*g* and 4°C, precipitated the collagen. After overnight redissolution in 10 m*M* HCl the material was dialyzed against 20 m*M* phosphate buffer for at least 8 hr at room temperature. Subsequent dialysis was performed against 20 m*M* phosphate buffer at 4°C for at least 8 hr and against 10 m*M* HCl at 4°C overnight. The resulting MRTC solution was stored at 4°C for the short-term or frozen and lyophilized.

Production of a Synthetic Collagen Microfiber by Continuous Coextrusion

A modified wet spinning device facilitated collagen fiber production (Figure 1). A collagen solution (2, 5, or 7.5 mg/mL in 10 m*M* HCl) and wet spinning buffer [(WSB): 10 wt% poly (ethylene glycol)] M_w = 35,000, 4.14 mg/mL monobasic sodium phosphate, 12.1 mg/mL dibasic sodium phosphate, 6.86 mg/mL TES (*N*-tris (hydroxymethyl) methyl-2-aminoethane sulfonic acid sodium salt), 7.89 mg/mL sodium chloride, pH 8.0) were extruded with a dual syringe pump

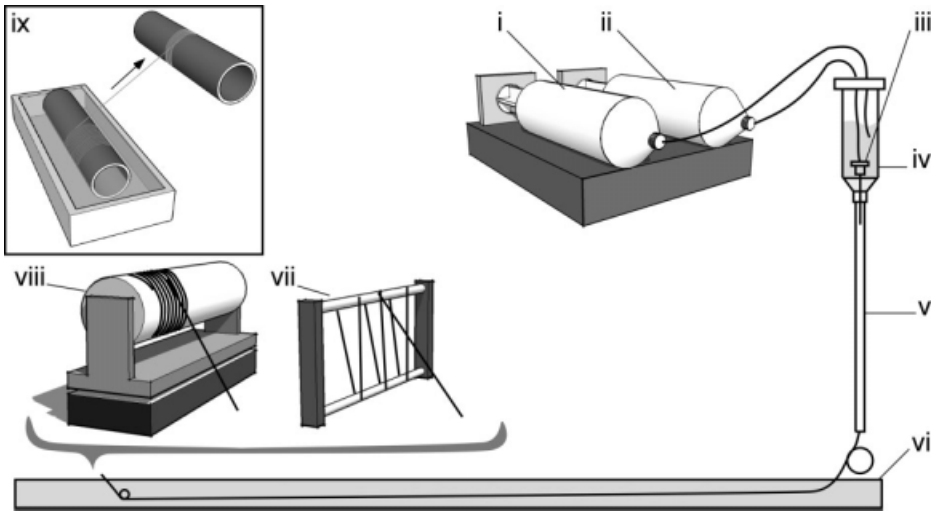

Figure 1. Wet spinning system. A syringe pump extruded WSB (i) though a bubble trap (iv) and into a coagulation column (v). The pump also drove the flow of the collagen solution (ii) through a spinneret (iii) and into the column. As the collagen stream emerged from the needle, it aggregated into a gel-like fiber due to the surrounding WSB. Flowing WSB carried the collagen fiber down the column, into the 70% ethanol rinse (vi). Short fiber segments were collected from the rinse with a hand-operated frame (vii). An automated carrier cylinder system (viii) was installed to collect 30 to 60 m of continuous fiber. After phosphate buffer incubation and rinsing, fiber was dried by transferring to a second carrier cylinder (ix). Draw ratios corresponding to the 70% ethanol rinse (vi) and the automated drying process (ix) were calculated.

(Harvard Apparatus, Holliston, MA). The collagen solution emerged through a 0.1 or 0.4 mm inner diameter spinneret into the center of a vertical tube (1.6 mm inner-diameter $\times$ 1 m long fluoropolymer tubing) at rates 0.03, 0.06, 0.08, or 0.1 mL/min. WSB simultaneously advanced through a bubble trap and down the fluoropolymer tube at a rate of 1.0 mL/min. As it exited the spinneret, the collagen coagulated into a gel-like fiber and traveled downward with the WSB stream.

Upon emergence from the fluoropolymer tube, the fiber entered a 2 meter-long rinsing bath of 70% ethanol in water. Initially, 5 to 10 m fiber samples were manually collected (MC) by winding onto rectangular frames. After optimization, automatically collected (AC) fiber was produced and collected onto a polyvinyl chloride carrier cylinder that rotated and translated automatically. During AC fiber production, carrier cylinders (outer diameter 48 mm) were typically rotated at 6 rpm and translated at 6 mm/minute, leading to the deposition of consecutive loops of 15.2 cm of fiber along the 20 cm length of the cylinder. The rate of fiber production was 60 m/hr.

Fiber Incubation and Drying

After spinning, the fiber was incubated in phosphate buffer (7.89 mg/mL sodium chloride, 4.26 mg/mL dibasic sodium phosphate, 10 m*M* Tris, pH 7.4) at 37°C for 48 hr.[25] MC fiber was incubated on rectangular frames, while AC fiber was incubated directly on the carrier cylinder. Rectangular frames containing MC were subsequently rinsed for 15 min in ddH20 and 2 min in 70% ethanol before drying in air. Carrier cylinders containing AC fiber were rinsed in ddH20 for 15 min before drying and collecting the fiber under tension with an automated system (Figure 1).

Fiber Crosslinking

Some fibers were left in a desiccator on a ceramic plate above a pool of 25% (w/v) glutaradehyde in water for 18 to 24 hr. To remove excess glutaraldehyde, fibers were subjected to three 4 hr rinses, gently rocking in PBS. Fibers were stored in PBS for immediate testing or rinsed in water and air-dried.

Optimization of Wet Spinning Parameters

During the course of MC production, collagen concentration, solution flow rate, and the dimensions of the spinneret were varied. For each set of parameters, samples were subjected to vapor phase glutaraldehyde crosslinking. Fiber diameter and mechanical properties were measured for the different wet spinning parameter combinations to guide the selection of conditions for AC fiber production (Table I).

Mechanical Annealing of Collagen Fibers

Fiber was collected onto hand-operated expandable rectangular frames and incubated in phosphate buffer at 37°C for 24 hr. The expandable frame was, thereafter, adjusted to impart 0, 15, or 30% strain to the fibers followed by 24 hr incubation in phosphate buffer. These samples, referred to as MC-0%, MC-15%, and MC-30%, were rinsed and dried.

TABLE I. Wet Spinning Parameters[a]

MC Sample Number/AC	Spinneret Inner Diameter (mm)	Collagen Extrusion Rate (mL/min)	Collagen Concentration (mg/mL)
1	0.4	0.1	5
2	0.4	0.06	5
3	0.4	0.03	5
4	0.4	0.015	5
5	0.4	0.1	2
6	0.4	0.06	2
7	0.4	0.06	7.5
8	0.1	0.06	7.5
9	0.1	0.03	7.5
AC	0.4	0.08	5

[a] MC sample numbers 4–6 were not analyzed further because the low collagen extrusion rate or concentration resulted in frequent breaks during fiber spinning.

Fiber structure was analyzed by transmission electron microscopy (TEM).

Analysis of Fiber Diameter, Cross-Sectional Area, and Draw Ratio

Draw ratios were calculated indirectly, based upon fiber cross-sectional area changes, to describe the effect of imposed tension. The first draw ratio corresponded to tension applied as the fiber was pulled through the 70% ethanol bath, while the second corresponded to tension during the automated drying process. In the first case, the draw ratio was estimated from the ratio of the cross-sectional area of fiber that was collected on the carrier cylinder [Figure 1(viii)] to the area of fiber that was collected manually on a rectangular frame [Figure 1(vii)]. Fibers collected on the carrier cylinder were pulled through the ethanol bath, while those collected manually were directly deposited onto a rectangular frame without imposed tension or drawing through an ethanol bath and only then subsequently incubated for 2 min in 70% ethanol. The draw ratio due tension during the automated drying process [Figure 1(ix)] was estimated from the cross-sectional area of fiber collected onto a drying cylinder to the area of those fibers collected onto a rectangular frame. In the former instance, a fiber from a cylinder that had been initially incubated in phosphate buffer for 48 hrs was drawn from a 70% ethanol bath to a second cylinder for completion of the air-drying process. In the latter case, fiber was manually unwrapped from the carrier cylinder after incubation in phosphate buffer and rinsing in 70% ethanol onto a rectangular frame. The cross-sectional areas were calculated from the average of nine diameter measurements of dry fiber examined beneath a 40× objective.

In all cases, the fiber cross-section was flattened during phosphate buffer incubation. To describe the noncircular cross-section, nine measurements of the dried fiber major (D_{major}) and minor (D_{minor}) diameters were made with a 40× objective, and the cross-sectional area was calculated from the average dimensions using the formula for an ellipse [$A_{cross\text{-}section} = \pi\ (D_{major} \cdot D_{minor})/4$].

The cross-sectional area of hydrated, crosslinked fiber was similarly determined. Each fiber segment was hydrated for 2 hrs in PBS and examined under a 20× objective. Three separate measurements of the major (D_{major}) and minor (D_{minor}) diameters were recorded for each test specimen. After analyzing six to ten samples for each fiber type, the hydrated cross-sectional area was calculated, as described above.

Mechanical Responses of Single Collagen Fibers

A Dynamic Mechanical Thermal Analyzer V (DMTA V, Rheometric Scientific, Piscataway, NJ) was used to determine tensile mechanical properties of fiber samples. Either end of a dry fiber was secured between thin plastic shims of a test frame with cyanoacrylate glue. Samples were hydrated overnight in PBS, loaded in the DMTA with a gauge length of 6 to 9 mm, and submerged in PBS at 37°C. Samples were subjected to 5% strain in four preconditioning cycles and then strained to failure at 5 mm/min. Engineering ultimate tensile stress (UTS) was determined using the calculated hydrated cross-sectional area.

Microdifferential Scanning Calorimetry (μDSC)

AC fiber before or after the phosphate buffer incubation (AC-phos and AC+phos), AC fiber after incubation and glutaraldehyde crosslinking (AC+phos+GLUT), as well as rat tail tendon (RTT) were pressed into 5–8 mg pellets, dried under vacuum, massed, and hydrated for 10 hrs in 0.5 mL of PBS at 5°C. MRTC was tested in solution in 10 m*M* HCl at 1 mg/mL. The hydrated or dissolved samples were heated in a μDSC III (Setaram Instrumentation, Caluire, France) from 5 to 90°C at 0.5°C/min and then cooled to 5°C. The denaturation temperature, T_m, and enthalpy of denaturation, ΔH, were determined from a plot of heat flow per unit mass as a function of temperature. The absence of a thermal transition in a second identical heating cycle confirmed complete denaturation in the initial heating cycle.

Microcalorimetry was also used to investigate residual poly(ethylene glycol) (PEG M_w 35,000) in the synthetic collagen fiber. Fiber samples were removed from the wet spinning system before entry into the 70% ethanol bath, after traveling through 0.2 m of the bath, and after the complete 2 m bath. Fiber was air dried and examined in the dry state to reveal the melting of PEG 35,000. Fiber specimens weighing 5 to 10 mg were analyzed with the μDSC III by heating from 20 to 70°C at 1.0°C/min.

Second Harmonic Generation (SHG) Microscopy

The second harmonic generation (SHG) system consisted of an Olympus IX71 inverted microscope coupled to a Ti-Sapphire laser (Spectra Physics, Mountain View, CA). A

60 × 1.2 NA (0.28 mm) water immersion objective focused and collected the backward signal, while a 1.4 NA oil immersion condenser (Olympus, Center Valley, PA) collected the forward signal. High sensitivity photomultiplier tube devices (Hamamatsu Photonics, Hamamatsu City, Japan) detected both the forward and backward signals. In preparation, noncrosslinked AC fiber was hydrated in PBS for 2 hrs and mounted beneath a cover slip with PVA-Dabco mounting media. Ten-micron cryosections of RTT were also mounted with PVA-Dabco. Spectrometer analysis of the emitted signal confirmed the presence of a steep intensity peak at 480 nm, half the excitation wavelength of 960 nm, indicative of SHG. The forward-to-backward (F/B) signal ratios were calculated for both RTT and synthetic collagen fiber test samples.

Transmission Electron Microscopy

Bundles of ~10 parallel, noncrosslinked fibers were tied at both ends with 4–0 prolene suture, hydrated for 1 hr in PBS, rinsed three times in 0.1 *M* cacodylate buffer (pH 7.4), fixed (2.5% glutaraldehyde in 0.1 *M* cacodylate buffer, pH 7.4) for 90 minutes, and washed in 0.1 *M* cacodylate water followed by ddH_20. Samples were partly dehydrated in 30% ethanol followed by staining en bloc with filtered 2% uranyl acetate in 50% ethanol. Preparation continued with ethanol series dehydration, 100% resin infiltration, and polymerization for 3 days at 60°C. Using an RMC MT-7000 ultramicrotome (Boeckeler, Tucson, AZ) and a diamond knife, ultrathin sections (60–80 nm) were cut to reveal cross and axial perspectives of the fiber interior. Following post-staining with 3% uranyl acetate and Reynold's lead citrate, sections were examined and photographed with a JOEL JEM-1210 TEM (JOEL, Tokyo, Japan) at 90 kV. Collagen fibril diameter was analyzed from 40 measurements taken from images of at least four different fiber cross-sections, magnified at 50,000×. Values were expressed as mean and standard deviation. Collagen fibril density was calculated by processing images of the fiber cross-section with ImageJ software.[26] Using the threshold function, 400 × 400 nm regions were converted to black and white and the percentage of black pixels was taken to represent fibril density. Three regions from three images of the fiber cross-section were analyzed.

Murine Subcutaneous Implant Studies

Fiber samples were implanted in the subcutaneous tissue of 10-week-old, 25–30 g, inbred male C57BL/6 mice (Jackson Laboratory, Bar Harbor, ME), as approved by the Emory University Institutional Animal Care and Use Committee. Bundles of 160 AC fibers, 1 cm in length, were aligned and tied at both ends with 7-0 prolene suture. Crosslinked bundles were exposed to glutaraldehyde vapor for 18 hr, followed by a 24 hr incubation in sterile water and a 1 hr incubation in PBS immediately before implantation. Noncrosslinked bundles were incubated in PBS for 1 hr immediately before implant. Five bundles of crosslinked and noncrosslinked fiber were implanted for a 6 week period.

Following sedation with ketamine (95 mg/kg, IM) and xylazine (5 mg/kg, IM), a subcutaneous pouch was created through a dorsal midline incision and the fiber bundle implanted. After 6 weeks, animals were sacrificed, fiber bundles were excised with overlying skin, and samples were photographed to qualitatively assess gross local tissue responses. All samples were fixed overnight in 10% neutral buffered formalin and processed for paraffin embedding. Five-micron sections were stained with Gomori's Trichrome to distinguish tissue morphology and collagen. The cross-sectional area of several representative crosslinked and noncrosslinked fibers from the bundle interior and periphery was measured with ImageJ software. The cross-sectional area of nonimplanted crosslinked and noncrosslinked fibers similarly sectioned and stained was measured. Immunohistochemical staining was performed with rat monoclonal antibody [CI:A3-1] which recognizes the F4/80 antigen expressed by murine macrophages (Abcam, Cambridge, MA).

Statistical Methods

Tests for statistically significant differences between the means of two groups were conducted with the Student's *t*-test (two-tailed, homoscedastic). Tests between three or more groups were conducted with one-way analysis of variance followed by the Tukey HSD test.

RESULTS

Collagen Fibers can be Produced Without Loss of Triple Helical Structure

The thermal characteristics of triple helical structure were quantified in terms of apparent enthalpy, ΔH, and temperature of denaturation, T_m. Collagen monomer T_m is a measure of triple helix stability, and is slightly below body temperature to allow micro unfolding during the assembly of collagen fibrils.[27] The enthalpy of collagen monomer unfolding corresponds to the energy required to disrupt factors including hydrogen bonding, steric, and electrostatic interactions.[28,29] The observed T_m and ΔH depend to varying degrees on experimental conditions, such as solution concentration, ionic strength, pH, and heating rate, and on factors, such as collagen aggregation or fibrillar assembly and the extent of covalent crosslinking. Results for monomeric collagen in solution, hydrated synthetic collagen fibers before and after phosphate buffer incubation, crosslinked synthetic fibers, and RTT are shown in Table II. Microcalorimetry revealed that before phosphate buffer incubation, the ΔH of synthetic fibers was similar to the dissolved monomer, while average T_m was increased by 8.4°C compared to the monomer solution (Table II, Figure 2). Phosphate buffer incubation increased ΔH of synthetic fiber to the level of RTT and slightly increased T_m. Sam-

TABLE II. Apparent Temperature and Enthalpy of Collagen Denaturation[a]

	MRTC	AC-Phos	AC + Phos	AC + Phos + GLUT	RTT
T_m (°C)	36.2 ± 0.6	44.8 ± 0.2	46.9 ± 1.7	78.6 ± 4.0	58.9 ± 0.4
ΔH (J/g)	49.4 ± 0.8	48.9 ± 2.1	57.4 ± 0.9	26.0 ± 3.6	56.3 ± 0.8

[a] Purified collagen (MRTC), automatically collected fiber without buffer treatment (AC-phos), with buffer treatment (AC + phos), after glutaraldehyde crosslinking (AC + phos + GLUT), and rat-tail tendon (RTT). Both the process of spinning collagen into fiber and the phosphate buffer incubation increased the thermal stability of the material, as shown by the elevated T_m and ΔH values. Values are the mean and standard deviation from three scans.

ples of RTT displayed a substantially higher T_m than non-crosslinked synthetic fiber samples. Glutaraldehyde crosslinking of synthetic fiber increased T_m above that of RTT, but lowered ΔH.

Microcalorimetry demonstrated the presence of PEG 35,000 in samples of synthetic fiber retrieved from the wet spinning system before entering the 2 m 70% ethanol rinse. Fiber that was rinsed for 0.2 m displayed a small transition corresponding to the melting of PEG 35,000, whereas fiber that was exposed to a 2 m length of the rinsing bath did not generate a detectable transition consistent with complete removal of residual PEG (Figure 3).

Synthetic Collagen Fiber Size and Strength

Between 8 and 18 specimens of each fiber type were evaluated for size and strength (Table III). Fiber diameter increased significantly ($p < 0.05$) with increasing collagen flow rate and collagen concentration (Figure 4). Increasing spinneret size by a factor of four did not significantly increase major diameter. The UTS of MC samples ranged between 54 and 90 MPa. Adjustment of any single spinning parameter in isolation did not produce statistically significant changes in fiber UTS (Figure 4). Nonetheless, MC sample 9 was stronger than samples 1, 2, and 7, and AC fiber displayed greater tensile strength than MC samples 1, 2, 7, and 8 (Table III). A typical stress–strain response of a single AC fiber is shown in Figure 5. The mass of dry AC fiber before crosslinking was 0.30 mg/m, while the mass after crosslinking was 0.33 mg/m.

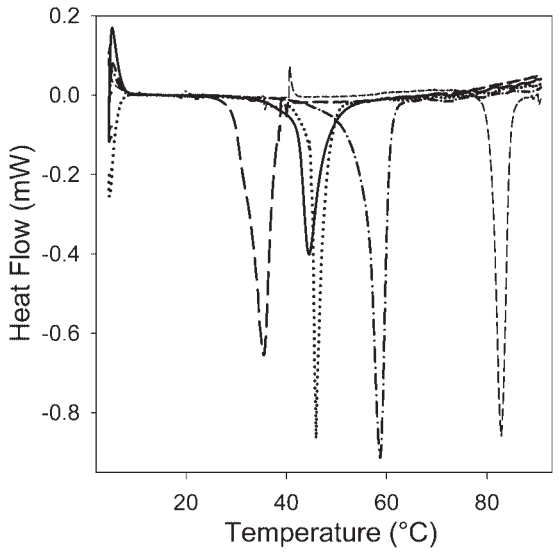

Figure 2. Microdifferential scanning calorimetry of MRTC (long dash), AC-phos (solid), AC+phos (dotted), RTT (dash-dot), and AC+phos+GLUT (short dash). Representative results from three experiments are shown.

Collagen Fibers can be Produced as a Close Packed Assembly of Axially Oriented D-Periodic Fibrils

D-periodic banded fibrils were observed in fiber samples that had been incubated in phosphate buffer, while nonincubated fiber displayed only thin, short, nonbanded fibrils (Figure 6). It is well known that collagen solutions can be reconstituted into D-periodic fibrils in the presence of monovalent salts, neutral pH, and warm temperatures.[30] However, in the current study phosphate buffer incubation converted collagen that was precipitated and dried without a pre-existing banded microstructure into fibrils that were uniformly D-periodic.

In the absence of axial loading (MC-0%), fibrils generated by the MC method were largely disorganized, but displayed a preferred axial alignment in the direction of loading when subjected to an imposed strain of 15 or 30% (Figure 7). In contrast, fibers produced by the AC method displayed aligned, densely packed fibrils (d 33 ± 4 nm) even in the absence of mechanical annealing (Figure 8). However, tensile strain was applied during the AC process, as demonstrated by the calculated draw ratios. The draw ratio corresponding to tension applied in the 2 m ethanol

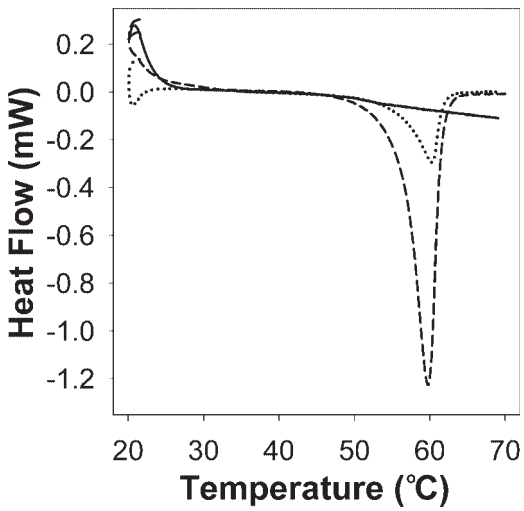

Figure 3. Microdifferential scanning calorimetry of synthetic fiber that was not rinsed in the 70% ethanol bath (dashed), rinsed in a 0.2 m bath (dotted), and a 2 m bath (solid).

TABLE III. Size and Mechanical Properties of Collagen Fiber[a]

MC Sample Number/AC[a]	Spinneret ID (mm)	Extrusion Rate (mL/min)	Concentration (mg/mL)	Major Diameter (mμ)	Minor Diameter (mμ)	UTS (MPa)	Modulus (MPa)	Strain-to-Failure (%)	n
1	0.4	0.1	5	59 ± 10	22 ± 3	54 ± 12	556 ± 120	11.2 ± 2.9	8
2	0.4	0.06	5	37 ± 9	17 ± 2	60 ± 16	529 ± 157	12.4 ± 3.1	7
3	0.4	0.03	5	25 ± 4	12 ± 2	77 ± 16	673 ± 100	12.6 ± 1.8	9
7	0.4	0.06	7.5	55 ± 6	27 ± 2	55 ± 14	575 ± 66	11.2 ± 2.5	12
8	0.1	0.06	7.5	44 ± 6	25 ± 2	67 ± 19	608 ± 54	12.2 ± 3.2	10
9	0.1	0.03	7.5	29 ± 3	20 ± 2	90 ± 37[b]	837 ± 133	11.7 ± 3.5	10
AC	0.4	0.08	5	53 ± 14	21 ± 3	94 ± 19[c]	775 ± 173	14.3 ± 1.9	18

[a] Samples 4 through 6 did not consistently produce fiber.
[b] The UTS of MC sample 9 was statistically greater than the UTS of the samples 1, 2, and 7 at the $p < 0.05$ level.
[c] The UTS of AC fiber was statistically greater than samples 1, 2, 7, and 8 at the $p < 0.05$ level.

rinse bath in the AC process was 1.5 (50% strain). The draw ratio corresponding to tension applied after buffer incubation was 1.0 (0% strain). The fibril density calculated for AC fiber was 73% ± 6% (v/v). SHG microscopy revealed signal generation in all regions of the fiber, confirming fibril formation throughout (Figure 9). The ratio of the forward-to-backward signal intensity, which is related, in part, to fibril diameter, was 0.039 for continuous fiber and 3.75 for rat-tail tendon.

Murine Subcutaneous Implant Studies

During the implant period, the length of noncrosslinked bundles decreased and the cross-sectional area of individual fibers increased, while crosslinked bundles maintained a constant length and fiber area. After 6 weeks, all samples were readily located and explanted. Noncrosslinked fiber bundles were firmly adherent to the overlying skin, while crosslinked bundles were not. Bundle length and fiber cross-sectional area were characterized with photography and histology. Photographic examination before and after implantation indicated that crosslinked fiber length was unchanged, while noncrosslinked fibers displayed a ~70% reduction in length (Figure 10). Gomori's Trichrome stained synthetic noncrosslinked fibers blue, similar to native collagen. Crosslinked fibers stained red, indicating that glutaraldehyde prevented the diffusion of Weigert hematoxylin from the fibers, as well as the uptake of the aniline blue counterstain. Among crosslinked fibers, the cross-sectional area of individual fibers was 460 ± 130 μm^2 at the bundle periphery and 440 ± 170 μm^2

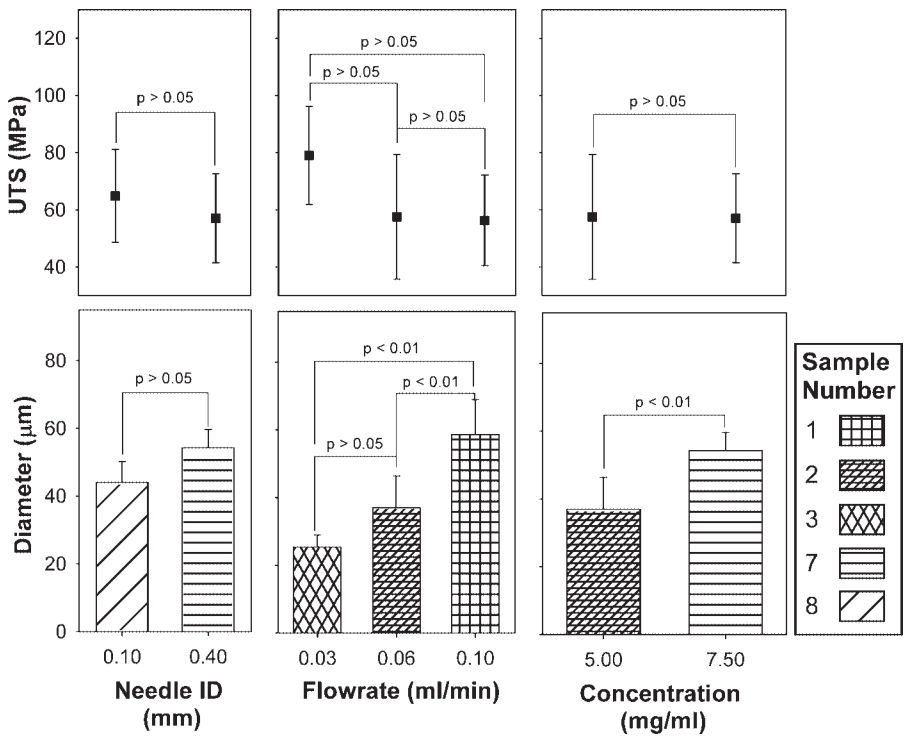

Figure 4. Mean UTS and major diameters of crosslinked MC fiber with varied wet spinning parameters. Sample numbers correspond to the parameters in Table I. Error bars represent standard deviations.

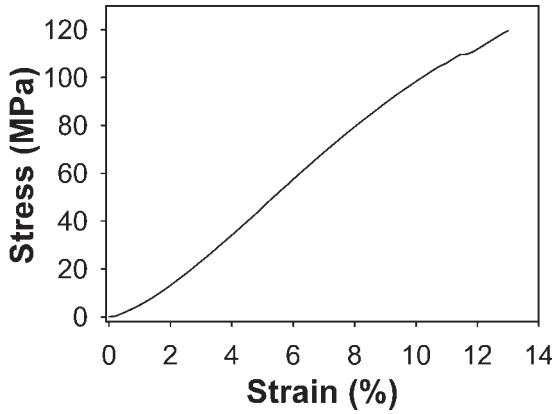

Figure 5. Representative stress–strain data for AC fiber.

in the bundle interior ($n = 15$). In contrast, noncrosslinked fiber areas were 340 ± 150 μm^2 at the periphery and 820 ± 340 μm^2 in the interior ($n = 22$). Nonimplanted fibers that were similarly sectioned and stained had areas of 470 ± 60 and 450 ± 40 μm^2 for noncrosslinked and crosslinked specimens ($n = 15$). The fibers in the interior of the noncrosslinked bundles were significantly larger than all other groups ($p < 0.01$).

Native collagen was deposited throughout the crosslinked fiber bundles, surrounding individual fibers or small fiber groups (Figure 11). In contrast, native collagen was deposited at the periphery of noncrosslinked bundles, with significantly less deposition in the bundle interior. Neovascularization was noted in the capsule surrounding noncrosslinked bundles and the in the interior of the crosslinked bundles. Similarly, cell infiltration was observed throughout the crosslinked bundle interior but was limited to the periphery of the noncrosslinked bundles. Immunohistochemistry demonstrated that macrophages were also predominantly at the perimeter of noncrosslinked bundles, and localized more uniformly throughout the crosslinked bundles (Figure 12).

DISCUSSION

Production of Continuous Synthetic Collagen Fiber

The progression of synthetic collagen fiber technology can be classified in terms of increasingly pure starting material. Initially, catgut suture was processed by segmenting ovine or bovine intestine into strips, rolling these into filaments, and polishing the filament to enhance uniformity. The fabrication also comprised of chemical processing, often including crosslinking with chromic trioxide.[31] However, localized tearing of the collagen fibril structure due to the manufacturing process was noted, leading to potential failure points.[31] Moreover, tissue reactivity to implanted suture often generated a highly inflammatory response.[32]

The subsequent set of technologies, reconstituted collagen fiber, consisted of the extrusion of partially purified collagen, in the form of fibril dispersions or slurries, into a coagulation bath followed by various dehydration and crosslinking steps. These processes were developed to improve thread uniformity and manufacturing efficiency and remove noncollagenous proteins, as well as polysaccharides, lipids, or cellular debris as potential antigenic, infectious, or inflammatory constituents. Specifically, tendon was processed into gels or dispersions consisting of collagen fibrils, extruded into

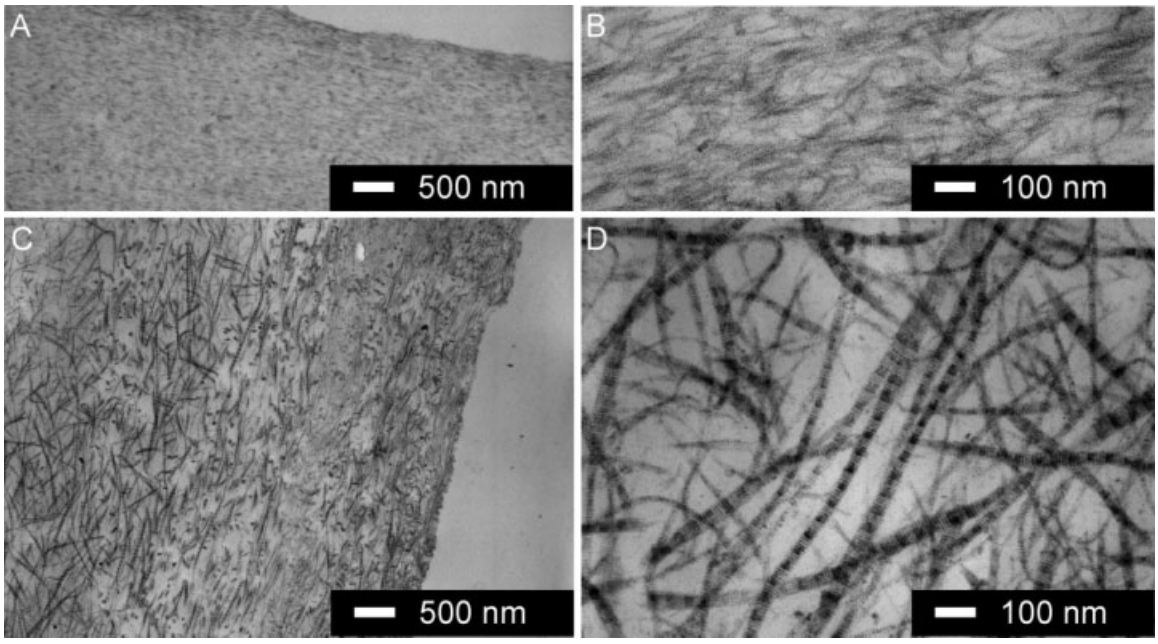

Figure 6. Incubation in phosphate buffer results in the assembly of collagen fibrils. D-periodic collagen fibrils were not visible in fibers in the absence of phosphate incubation (A, B), but were evident following treatment (C, D).

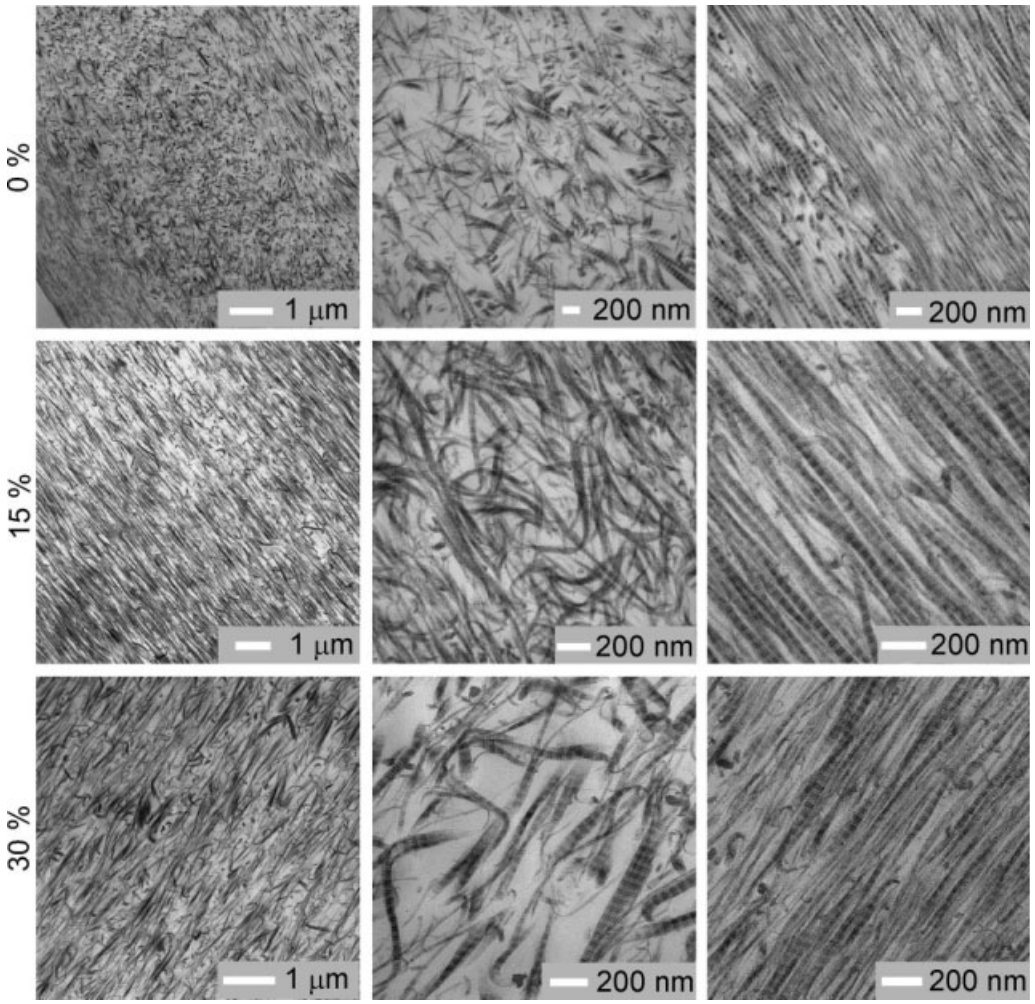

Figure 7. Mechanical annealing during incubation enhances fibril alignment. Lower magnification axial sections of MC-0%, MC-15%, and MC-30% (left column) showed a trend toward enhanced fibril alignment in the stretched samples (middle and bottom rows). Fibril diameters after 0, 15, and 30% strain were 30 ± 9, 31 ± 7, and 30 ± 6 nm (means and standard deviations from 40 measurements). Fibril alignment was not uniform: in high magnification images of the samples, regions of low fibril alignment (center column) and high alignment (right column) could be identified.

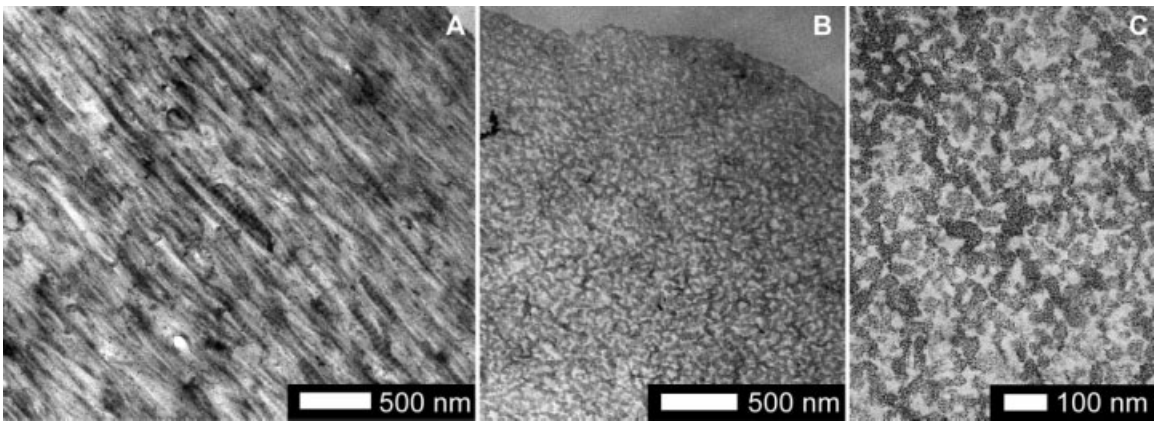

Figure 8. Fibrillar structure of phosphate buffer treated AC fiber imaged by TEM. Axial sections revealed an aligned pattern of fibrils, often displaying banding (A). Fiber cross sections consisted of tightly packed fibril cross sections (B, C). Samples were not crosslinked with glutaraldehyde vapor. Fibril diameters were 33 ± 4 nm (mean and standard deviation from 40 measurements).

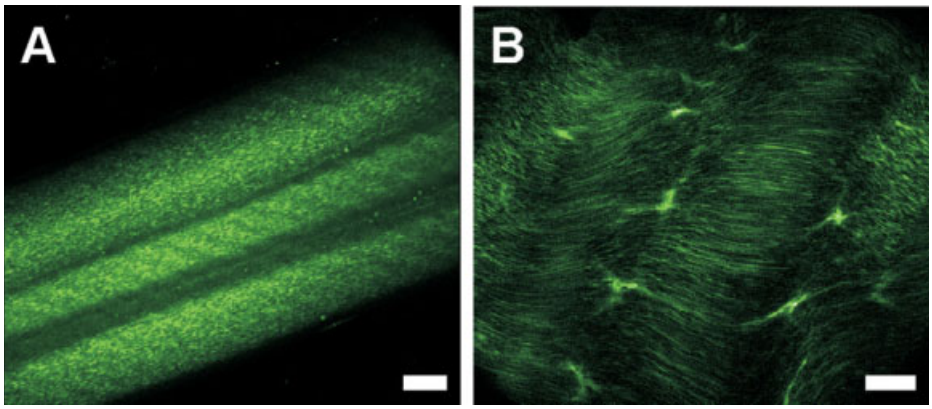

Figure 9. The second harmonic generated by phosphate buffer treated AC fiber and rat-tail tendon. A cluster of three wet spun fibers displayed a clear SHG signal but only short discontinuous fibrillar substructure was noted (A). The signal from rat-tail tendon revealed fibrillar structure (B). Scale bars are 20 μm. [Color figure can be viewed in the online issue, which is available at www.interscience.wiley.com.]

acetone-based solutions to precipitate fiber, and subject to a variety of crosslinking, mechanical drawing, and drying stages.[33,34] However, the performance of chromic crosslinked, reconstituted collagen fiber in animal studies was inferior when compared to chromic catgut due to suture fragmentation and chemical irritation.[35]

The most recent collagen fiber techniques have been based upon filtered solutions or dispersions of acid-extracted triple helical monomers or oligomers instead of fibrillar collagen.[36,37] In an attempt to avoid potentially denaturing solvents, such as acetone, during fiber processing, collagen was formulated into dispersions or solutions and extruded into aqueous buffers, followed by dehydration in alcohol, and air drying.[38] Although enhanced purity was achieved, scalability and control over fiber substructure remain limited. Specifically, these techniques either cannot produce large amounts of continuous fiber in a cost- and time-effective manner, or cannot replicate the structural features that dictate mechanical and biological properties. In synthetic collagen fiber, these structural features include the self-assembly of monomers into fibril building blocks; the generation of an aligned, axial fibril orientation; and the generation of uniform fibril formation throughout the fiber cross-section. Significantly, collagen fibril assembly, length, density, and alignment have been correlated to enhanced strength and viscoelastic properties.[39–41] Fibrillar assembly also modulates the capacity of collagenous materials to trigger gene expression. For example, compared directly to monomeric collagen, fibrillar collagen suppresses the expression of ECM molecules implicated in the smooth muscle cell response to injury.[42]

Strategies to Induce Molecular Assembly of Collagen to Reproduce the Fibril Substructure Observed in Native Collagen Fibers

The most recent fiber spinning methods have employed longer buffer incubations, ranging between 30 min[43] and 48 hr,[44] in order to allow monomer assembly into banded, fibril substructure. These incubation times facilitated the assembly of collagen molecules into fibrils, but fiber production was typically limited to discontinuous 10–20 cm segments. For example, Pins et al.[37,44] reported a discontinuous fiber process using longer incubation periods that generated fibrils throughout the fiber cross-section. In another discontinuous fiber system, Zeugolis et al.[43,45–47] recently demonstrated fibril formation after three incubations of 10 to 15 min.

Production of long, continuous fiber lengths that require extended buffer incubation periods has been deemed impractical. For example, if fiber was continuously extruded at 1 m/min with a requisite 30 minute incubation period, then 30 meters of the nascent protein filament would need to be threaded through a series of incubation baths without breaks or tangles. Thus, reported continuous fiber spinning systems

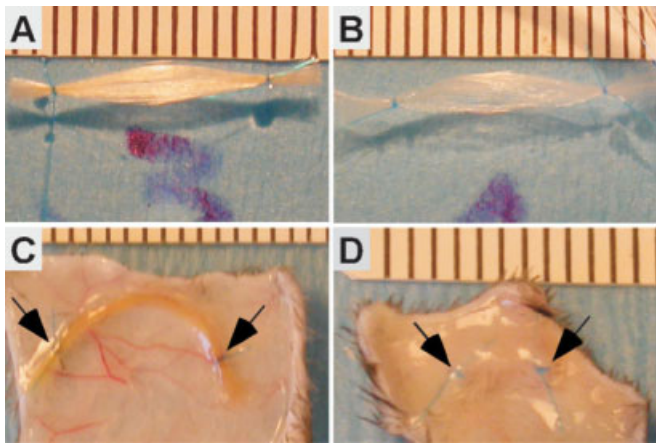

Figure 10. Photographs of fiber bundles before and after implant. Crosslinked and noncrosslinked bundles are shown immediately before the implant (A and B, respectively) and after retrieval (C and D, arrows indicate suture at the bundle ends). Crosslinked bundles maintained a similar size while noncrosslinked bundles consistently appeared smaller. Scale in mm. [Color figure can be viewed in the online issue, which is available at www.interscience.wiley.com.]

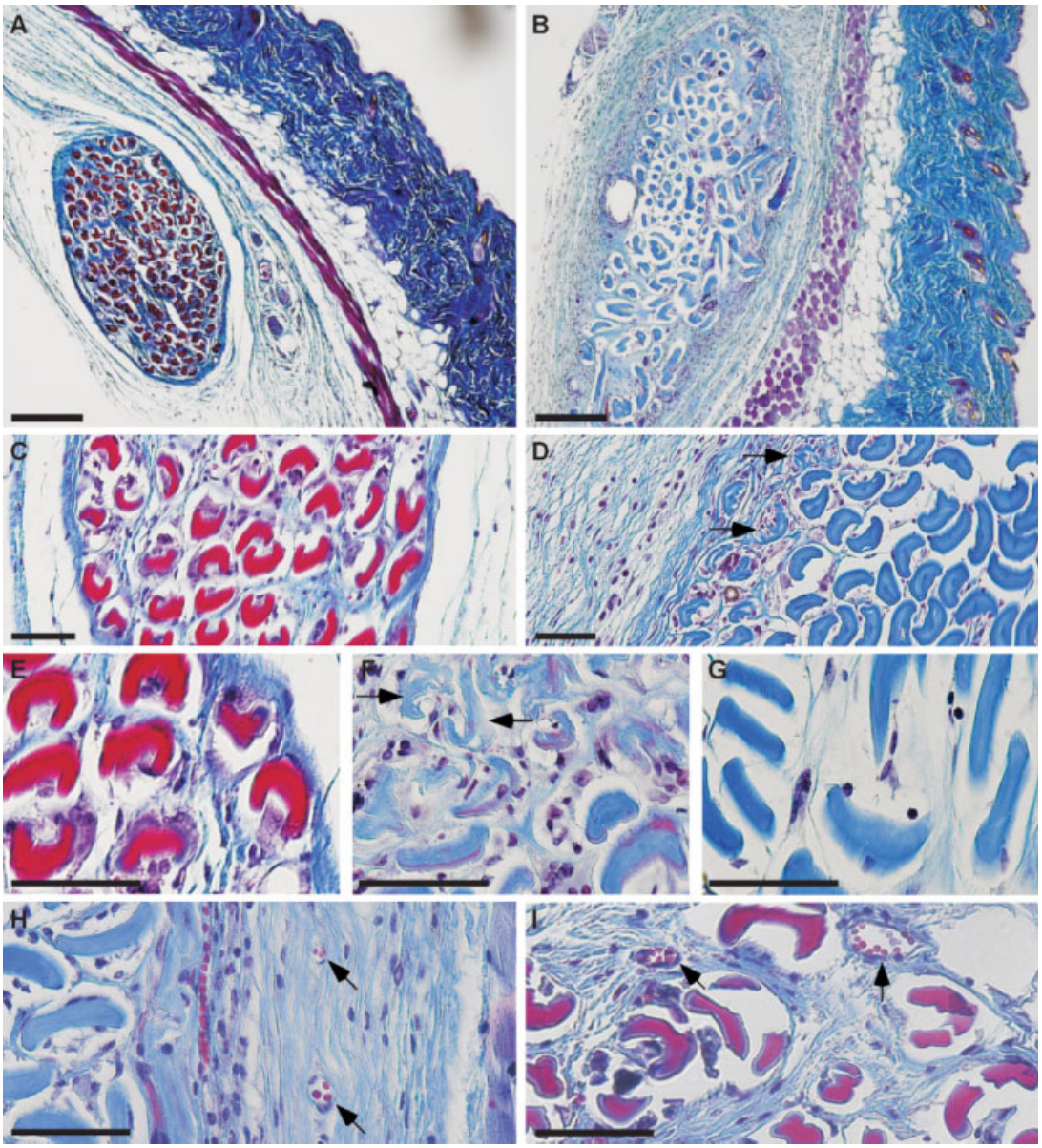

Figure 11. Morphology of explanted fiber bundles stained with Gomori's Trichrome. Crosslinked synthetic fibers (A, C, E, I) appeared red, while noncrosslinked synthetic fibers were blue (B, D, F, G, H). Deposition of native collagen fibers (blue) was more uniform throughout the crosslinked bundles, as seen in panels (A, C, E, and I). Collagen was deposited more densely around the periphery and less in the center of noncrosslinked bundles (B). At the periphery of noncrosslinked bundles (F and the left side of D), synthetic collagen fibers appeared smaller compared to fibers in the bundle center (G and right side of D). Many fibers at the periphery of noncrosslinked bundles displayed irregular borders (arrows in D and F). Vascularization was noted in the capsule surrounding noncrosslinked bundles, and in the interior of crosslinked bundles (arrows in H and I). Original magnifications were ×40 in A and B (scale 200 μm), ×200 in (C and D) (scale 50 μm), and ×400 in E, F,H, and I (scale 50 μm). [Color figure can be viewed in the online issue, which is available at www.interscience.wiley.com.]

have incorporated only brief incubation periods during fiber production.[48–50] In this regard, Silver and Kato[48] compared discontinuous and continuous methods and observed that fiber produced by a continuous process displayed inferior mechanical properties and an accelerated rate of biodegradation. Likewise, Cavallaro et al.[49] noted D-periodic collagen fibrils only on the outer shell of fibers produced by a continuous spinning method, consistent with the inferior mechanical and biological properties observed by Silver and Kato.

In this report, a purified, acid-extracted solution of monomeric collagen and a buffered PEG solution were continuously coextruded through fluoropolymer tubing to form a synthetic collagen fiber. The two-stage process that was designed decoupled the fiber extrusion process from a prolonged incubation step, thereby permitting both scalable pro-

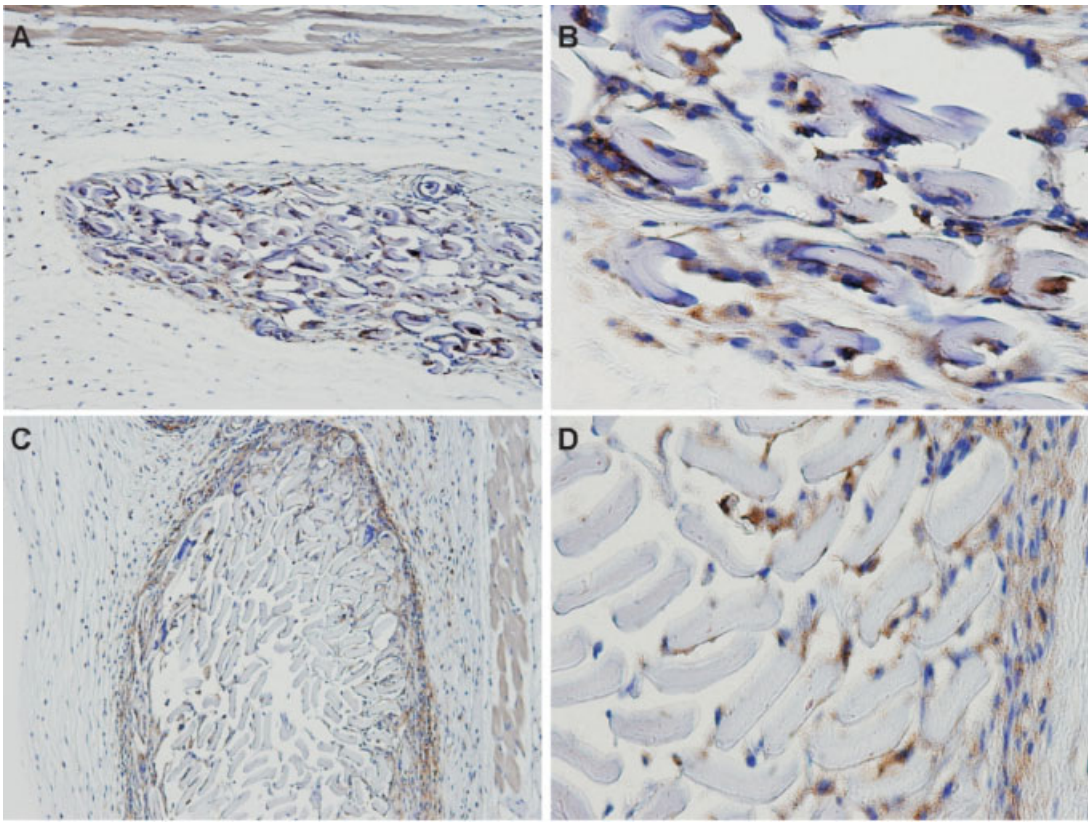

Figure 12. Macrophage distribution in crosslinked and noncrosslinked fiber bundles. Macrophages were present inside the crosslinked bundles of fiber (A, ×100, and B, ×400) but collected primarily around the perimeter of the noncrosslinked bundles (C, ×100, and D, ×400). [Color figure can be viewed in the online issue, which is available at www.interscience.wiley.com.]

duction and the development of optimal fibril substructure. Significantly, laboratory-scale continuous fiber production rates of 60 m/hr were achieved. Collagen assembly, denoted by the presence of aligned, D-periodic fibrillar substructure was observed by TEM. These data are consistent with the results of microcalorimetry studies and SHG microscopy, confirming the presence of collagen fibrils over large length scales. Enhanced mechanical properties were commensurate with the formation of close packed, D-periodic fibrils. MC fibers displayed a high degree of axial fibril alignment upon application of a mechanical annealing protocol, similar to the technique reported by Pins et al.[37] However, AC fiber displayed axial fibril alignment without additional mechanical stretching, which we attribute to the 1.5 draw ratio resulting from tension applied in the 2 m ethanol bath. The draw ratio corresponding to the automated drying process following phosphate incubation was 1.0. Thus, no additional strain was imparted during this step.

Calorimetric Analysis Demonstrates Conservation of Collagen Triple Helical Structure

Triple helical structure defines the collagen family of proteins, is a prerequisite for fibril self-assembly, and, critically, shields antigenic and proteolytic cleavage sites.[14] Use of unsuitable solvents and high temperatures, such as acetone in early collagen wet spinning processes and trifluoroethanol in collagen electrospinning,[51] destabilizes the triple helix and may compromise biocompatibility, biostability, and fiber strength. In this report, microcalorimetry demonstrated that spinning monomeric collagen into fibers, before fibrillogenesis, did not disrupt triple helical structure, with an increase in the observed T_m from 36.2 to 44.8°C. This increase may be attributable to enhanced stability of aggregated collagen in the fiber, as compared to monomeric collagen in solution. However, use of different solution compositions during calorimetry may also contribute to an observed difference in T_m. Specifically, synthetic fibers were hydrated in PBS (pH 7.4), while monomeric collagen was dissolved in 10 m*M* HCl (pH 2.0). The stability of the triple helix is related to pH, and increasing pH from 2 to 7.4 would account for an increase in T_m of ~2°C.[27,52] After fibrillogenesis, D-periodic fibril formation led to an increase in both T_m and ΔH. Enhanced thermal stability is likely due to increased hydrophobic interactions and surface energy associated an extensively, self-assembled, close packed fibrillar structure.[52] The T_m of AC fiber after phosphate incubation was 12°C less than that noted for native tendon, stabilized by native covalent crosslinks. However, after glutaraldehyde crosslinking, the T_m of synthetic fiber was 20°C greater than native tendon. The enthalpy of denaturation was substantially decreased after synthetic fiber crosslinking, due to additional covalent cross-

TABLE IV. Summary of Collagen Fiber Diameter and Strength in Prior Reports and in the Current Study[a]

Ref.	Continuous/ Discontinuous	Diameter (μm)	UTS (MPa)	Crosslinking Scheme[b]
38	D	–	66.2 ± 17.20 (Wet)	Glut vapor
48	C	70.3 ± 8.6 (Wet), 56.8 ± 7.4 (Dry)	36.9 ± 7.90 (Wet)	Glut vapor
59	D	20–40 (Dry)	42.9 ± 9.55 (Wet)	Glut vapor
36	D	–	91.8 ± 31.4 (Wet)	DHT
44	D	55.5 ± 5.17 (Dry), 88.72 ± 8.57 (Wet)	56.62 ± 11.17 (Wet)	DHT
43	D	52 ± 8 (Dry)	255 ± 89 (Dry)	None
47	D	153 ± 7 (Dry), 270 ± 8 (Wet)	182 ± 18 (Dry) 5.86 ± 1.01 (Wet)	None
46	D	119 ± 15 (Dry)	208 ± 57 (Dry)	None
45	D	306 ± 29 (Wet)	10.85 ± 2.85 (Wet)	Glut solution
49	C	25 (Dry)	27.7 ± 23.1 (Wet)	Glut vapor
Current study	C	53 ± 14 by 21 ± 3 (Wet) 21 ± 3 by 15 ± 1 (Dry)	93.9 ± 19.2 (Wet)	Glut vapor

[a] The strength of hydrated, glutaraldehyde crosslinked fibers is provided when available.

[b] L refers to crosslinking method and Glut, DHT, and EDC refer to glutaraldehyde, dehydrothermal, and 1-Ethyl-3-[3-dimethylaminopropyl]carbodiimide hydrochloride crosslinking. Glut and DHT refer to glutaraldehyde and dehydrothermal crosslinking.

links, which break exothermically upon denaturation, and a reduction in hydrogen bonds, which break endothermically.[53]

SHG Microscopy Confirms Retention of Triple Helical Structure and Fibril Assembly

SHG occurs when laser light passes through a molecularly noncentrosymmetric, highly polarizable material. The wavelength is halved and the frequency doubled in a coherent optical process.[54] Zeugolis et al.[51] demonstrated that the presence of SHG in extruded collagen fiber confirmed the retention of triple helical structure while the absence of SHG in collagen electrospun from denaturing solvents corresponded to the loss of triple helical structure. However, in addition to triple helical structure, collagen monomers must be assembled into fibrils to generate an SHG signal. For example, triple-helical, nonfibrillar collagen (type IV) does not produce SHG.[55,56] Furthermore, reports have proposed that only a portion of the collagen in a fibril, possibly in the fibril's outer shell, can generate SHG scattering.[8,57] The magnitude of SHG forward to backward signal ratios has been correlated with increased collagen fibril diameter. Presumably, forward signal accumulates as light travels through the fibril with limited backward signal summation due to destructive interference.[8] In this report, the F/B ratio observed for synthetic fibers was less than that of native RTT, consistent with smaller fibril diameters. Fibril diameters in synthetic fibers were 33 ± 4 nm, while fibril diameters in RTT have a bimodal distribution with average diameters of 70 and 250 nm.[58]

Fiber Diameter and Strength

Reduction of solution flow rate or collagen concentration resulted in a decrease in fiber diameter due to a reduction in mass flow rate. Reducing the spinneret diameter by a factor of four without adjustment to the collagen mass flow rate led to only a small reduction of fiber diameter. While the diameter of hydrated fiber produced by other strategies have ranged from 50 to 300 μm, we observed fibers as small as 12 to 25 μm in cross-section (Table IV). Significantly, the ultimate tensile strength of AC fiber is two to three times greater than that reported for other continuously spun fiber schemes (Table IV).

Local Tissue Responses to Collagen Fibers

A mild local inflammatory response was noted, consistent with previous reports of glutaraldehyde crosslinked synthetic collagens fiber implanted in rats and rabbits.[59,60] Over the 6-week implant period, crosslinked fibers displayed little change in length or morphology. Noncrosslinked fibers displayed significant reduction in length, an increase in the cross-sectional area of interior fibers, and little overall change in the area of peripheral fibers. The increase in the area of interior fibers may be due to swelling during the implant period. The reduced area of fibers at the bundle periphery compared to interior fibers, as well as the uneven cross-section of the peripheral fibers themselves, may indicate degradation of peripheral fibers. In comparison, synthetic collagen fibers produced by alternate schemes have exhibited more significant degradation even after chemical crosslinking. For example, after dehydrothermal-cyanamide crosslinking, Law et al.[59] noted that most fibers had degraded within 10 days, with complete loss after 6 week following intramuscular implantation in a rat model. Similarly, Kato and Silver[48] noted that crosslinked collagen fiber bundles degraded 2 week after subcutaneous implantation in the rat. The high degree of fibril alignment and close packed structure throughout the fiber may contribute to the observed enhancement in fiber stability.

CONCLUSIONS

Synthetic collagen fiber that closely mimics its native counterpart is a critical component in the engineering of tissue

replacements designed to couple the remodeling capacity of native ECM scaffolds with the structural definition afforded by textile or fiber-composite manufacturing. We report a laboratory-scale system that produced continuous synthetic collagen fiber at 60 m/hr from a monomeric collagen solution. In contrast to previously reported continuous fiber spinning systems, TEM and SHG revealed the assembly of D-periodic fibrils throughout the fiber cross-section. Moreover, tension maintained during automated fiber collection corresponded to the production of a highly aligned fibril structure and an ultimate tensile strength two to three times greater than reported for other continuous fiber processes. Adjustment of spinning parameters afforded controlled adjustment of major fiber diameter. Limited inflammatory response was observed in vivo with a relatively high degree of fiber biostability even in the absence of chemical crosslinking.

REFERENCES

1. Kielty C, Hopkinson I, Grant M. Collagen: The collagen family: Structure, assembly, and organization in the extracellular matrix. In: Royce P, Steinmann B, editors. Connective Tissue and its Heritable Disorders. Molecular, Genetic, and Medical Aspects. New York: Wiley-Liss; 1993. pp 103–147.
2. Canty EG, Kadler KE. Procollagen trafficking, processing and fibrillogenesis. J Cell Sci 2005;118 (Part 7):1341–1353.
3. Hulmes DJ. Building collagen molecules, fibrils, and suprafibrillar structures. J Struct Biol 2002;137:2–10.
4. Kadler KE, Hill A, Canty-Laird EG. Collagen fibrillogenesis: Fibronectin, integrins, and minor collagens as organizers and nucleators. Curr Opin Cell Biol 2008;20:495–501.
5. Ottani V, Martini D, Franchi M, Ruggeri A, Raspanti M. Hierarchical structures in fibrillar collagens. Micron 2002;33: 587–596.
6. Kadler KE, Holmes DF, Trotter JA, Chapman JA. Collagen fibril formation. Biochem J 1996;316 (Part 1):1–11.
7. Gutsmann T, Fantner GE, Venturoni M, Ekani-Nkodo A, Thompson JB, Kindt JH, Morse DE, Fygenson DK, Hansma PK. Evidence that collagen fibrils in tendons are inhomogeneously structured in a tubelike manner. Biophys J 2003;84: 2593–2598.
8. Chu S, Tai S, Chan M, Sun C, Hsiao I, Lin C, Chen YC, Lin B. Thickness dependence of optical second harmonic generation in collagen fibrils. Optics Express 2007;15:12005–12010.
9. Birk DE, Fitch JM, Babiarz JP, Doane KJ, Linsenmayer TF. Collagen fibrillogenesis in vitro: Interaction of types I and V collagen regulates fibril diameter. J Cell Sci 1990;95 (Part 4): 649–657.
10. Keene DR, Oxford JT, Morris NP. Ultrastructural localization of collagen types II, IX, and XI in the growth plate of human rib and fetal bovine epiphyseal cartilage: Type XI collagen is restricted to thin fibrils. J Histochem Cytochem 1995;43:967–979.
11. Hirsch M, Prenant G, Renard G. Three-dimensional supramolecular organization of the extracellular matrix in human and rabbit corneal stroma, as revealed by ultrarapid-freezing and deep-etching methods. Exp Eye Res 2001;72:123–135.
12. Ottani V, Raspanti M, Ruggeri A. Collagen structure and functional implications. Micron 2001;32:251–260.
13. Fung Y. Biomechanics: Mechanical Properties of Living Tissues. New York: Springer-Verlag; 1993.568 p.
14. Lynn AK, Yannas IV, Bonfield W. Antigenicity and immunogenicity of collagen. J Biomed Mater Res B Appl Biomater 2004;71:343–354.
15. Badylak SF. The extracellular matrix as a scaffold for tissue reconstruction. Semin Cell Dev Biol 2002;13:377–383.
16. Nelson CM, Bissell MJ. Of extracellular matrix, scaffolds, and signaling: Tissue architecture regulates development, homeostasis, and cancer. Annu Rev Cell Dev Biol 2006;22:287–309.
17. Guido S, Tranquillo RT. A methodology for the systematic and quantitative study of cell contact guidance in oriented collagen gels. Correlation of fibroblast orientation and gel birefringence. J Cell Sci 1993;105 (Part 2):317–331.
18. Cheng X, Gurkan UA, Dehen CJ, Tate MP, Hillhouse HW, Simpson GJ, Akkus O. An electrochemical fabrication process for the assembly of anisotropically oriented collagen bundles. Biomaterials 2008;29:3278–3288.
19. Hughes K, Hutson T, Fink J. Battell Development Corporation, assignee. Collagen Orientation, US Patent 4,544,516, 1985.
20. Yang C, Hillas PJ, Baez JA, Nokelainen M, Balan J, Tang J, Spiro R, Polarek JW. The application of recombinant human collagen in tissue engineering. BioDrugs 2004;18:103–119.
21. Wright E, McMillan R, Cooper A, Apkarian RP, Conticello VP. Thermoplastic elastomer hydrogels via self-assembly of an elastim-mimetic triblock polypeptide. Adv Funct Mater 2002;12:149–154.
22. Nagapudi K, Brinkman WT, Thomas BS, Park JO, Srinivasarao M, Wright E, Conticello VP, Chaikof EL. Viscoelastic and mechanical behavior of recombinant protein elastomers. Biomaterials 2005;26:4695–4706.
23. Rele S, Song Y, Apkarian RP, Qu Z, Conticello VP, Chaikof EL. D-periodic collagen-mimetic microfibers. J Am Chem Soc 2007;129:14780–14787.
24. Silver FH, Trelstad RL. Type I collagen in solution-structure and properties of fibril fragments. J Biol Chem 1980;255: 9427–9433.
25. Pins GP, Christiansen DL, Patel R, Silver FH. Self-assembly of collagen fibers. Influence of fibrillar alignment and decorin on mechanical properties. Biophys J 1997;73:2164–2172.
26. Abramoff M, Magelhaes P, Ram S. Image processing with ImageJ. Biophotonics Int 2004;11:36–42.
27. Leikina E, Mertts MV, Kuznetsova N, Leikin S. Type I collagen is thermally unstable at body temperature. Proc Natl Acad Sci USA 2002;99:1314–1318.
28. McClain PE, Wiley ER. Differential scanning calorimeter studies of the thermal transitions of collagen. Implications on structure and stability. J Biol Chem 1972;247:692–697.
29. Komsa-Penkova R, Koynova R, Kostov G, Tenchov BG. Thermal stability of calf skin collagen type I in salt solutions. Biochim Biophys Acta 1996;1297:171–181.
30. Gross J. The behavior of collagen units as a model in morphogenesis. J Biophys Biochem Cytol 1956;2 (Suppl 4):261–274.
31. Chu C. Chemical structure and manufacturing processes. In: Chu C, Fraunhofer J, Greisler H, editors. Wound Closure Biomaterials and Devices. Boca Raton, FL: CRC Press; 1996.
32. Hirko M, Lin P, Greisler H, Chu C. Biological properties of suture materials. In: Chu C, Fraunhofer J, Greisler H, editors. Wound Closure Biomaterials and Devices. Boca Raton, FL: CRC Press; 1996.
33. Salo T, Waugh D;Research Corporation, assignee. Preparation of collagenous materials, US Patent 2,598,608. 1946.
34. Griset E, Reissmann T, Brook B, Nichols J;Ethicon, Inc., assignee. Method of producing a collagen strand, US Patent 3,114,593, 1964.
35. Reynolds BL. Reconstituted collagen and chromic catgut suture for colon anastomoses in dogs. JAMA 1966;195:807–812.

36. Wang MC, Pins GD, Silver FH. Collagen fibres with improved strength for the repair of soft tissue injuries. Biomaterials 1994;15:507–512.
37. Pins G, Huang E, Christiansen D, Silver F. Effects of static axial strain on the tensile properties and failure mechanisms of self-assembled collagen fibers. J Appl Polym Sci 1997;63: 1429–1440.
38. Kato YP, Christiansen DL, Hahn RA, Shieh SJ, Goldstein JD, Silver FH. Mechanical properties of collagen fibres: A comparison of reconstituted and rat tail tendon fibres. Biomaterials 1989;10:38–42.
39. Silver FH, Freeman JW, Seehra GP. Collagen self-assembly and the development of tendon mechanical properties. J Biomech 2003;36:1529–1553.
40. Buehler MJ. Nature designs tough collagen: Explaining the nanostructure of collagen fibrils. Proc Natl Acad Sci USA 2006;103:12285–12290.
41. Roeder BA, Kokini K, Sturgis JE, Robinson JP, Voytik-Harbin SL. Tensile mechanical properties of three-dimensional type I collagen extracellular matrices with varied microstructure. J Biomech Eng 2002;124:214–222.
42. Ichii T, Koyama H, Tanaka S, Kim S, Shioi A, Okuno Y, Raines EW, Iwao H, Otani S, Nishizawa Y. Fibrillar collagen specifically regulates human vascular smooth muscle cell genes involved in cellular responses and the pericellular matrix environment. Circ Res 2001;88:460–467.
43. Zeugolis DI, Paul RG, Attenburrow G. Factors influencing the properties of reconstituted collagen fibers prior to self-assembly: Animal species and collagen extraction method. J Biomed Mater Res A 2008;86:892–904.
44. Pins GD, Christiansen DL, Patel R, Silver FH. Self-assembly of collagen fibers. Influence of fibrillar alignment and decorin on mechanical properties. Biophys J 1997;73:2164–2172.
45. Zeugolis DI, Paul GR, Attenburrow G. Cross-linking of extruded collagen fibers-A biomimetic three-dimensional scaffold for tissue engineering applications. J Biomed Mater Res A 2009;89: 895–908.
46. Zeugolis DI, Paul GR, Attenburrow G. Engineered extruded collagen fibers for biomedical applications. J Appl Polym Sci 2008;108:2886–2894.
47. Zeugolis DI, Paul RG, Attenburrow G. Post-self-assembly experimentation on extruded collagen fibres for tissue engineering applications. Acta Biomater 2008;4:1646–1656.
48. Kato YP, Silver FH. Formation of continuous collagen fibres: Evaluation of biocompatibility and mechanical properties. Biomaterials 1990;11:169–175.
49. Cavallaro J, Kemp P, Kraus K. Collagen fabrics as biomaterials. Biotechnol Bioeng 1994;43:781–791.
50. Fofonoff T, Bell E;Tissue Engineering, Inc., assignee. Apparatus and method for spinning and processing collagen fiber, US Patent 5,562,946, 1996.
51. Zeugolis DI, Khew ST, Yew ES, Ekaputra AK, Tong YW, Yung LY, Hutmacher DW, Sheppard C, Raghunath M. Electro-spinning of pure collagen nano-fibres—Just an expensive way to make gelatin? Biomaterials 2008;29:2293–2305.
52. Wallace DG, Condell RA, Donovan JW, Paivinen A, Rhee WM, Wade SB. Multiple denaturational transitions in fibrillar collagen. Biopolymers 1986;25:1875–1895.
53. Bigi A, Cojazzi G, Panzavolta S, Rubini K, Roveri N. Mechanical and thermal properties of gelatin films at different degrees of glutaraldehyde crosslinking. Biomaterials 2001;22: 763–768.
54. Campagnola PJ, Loew LM. Second-harmonic imaging microscopy for visualizing biomolecular arrays in cells, tissues and organisms. Nat Biotechnol 2003;21:1356–1360.
55. Brown E, McKee T, diTomaso E, Pluen A, Seed B, Boucher Y, Jain RK. Dynamic imaging of collagen and its modulation in tumors in vivo using second-harmonic generation. Nat Med 2003;9:796–800.
56. Zipfel WR, Williams RM, Christie R, Nikitin AY, Hyman BT, Webb WW. Live tissue intrinsic emission microscopy using multiphoton-excited native fluorescence and second harmonic generation. Proc Natl Acad Sci USA 2003;100:7075–7080.
57. Williams RM, Zipfel WR, Webb WW. Interpreting second-harmonic generation images of collagen I fibrils. Biophys J 2005;88:1377–1386.
58. Parry DA, Craig AS. Quantitative electron microscope observations of the collagen fibrils in rat-tail tendon. Biopolymers 1977;16:1015–1031.
59. Law JK, Parsons JR, Silver FH, Weiss AB. An evaluation of purified reconstituted type 1 collagen fibers. J Biomed Mater Res 1989;23:961–977.
60. Kato YP, Dunn MG, Zawadsky JP, Tria AJ, Silver FH. Regeneration of Achilles tendon with a collagen tendon prosthesis. Results of a one-year implantation study. J Bone Joint Surg Am 1991;73:561–574.